Speciation, Characterization, and Mobility of As, Se, and Hg in Flue Gas Desulphurization Residues

ARTICLE *in* ENVIRONMENTAL SCIENCE AND TECHNOLOGY · APRIL 2008

Impact Factor: 5.33 · DOI: 10.1021/es702479n · Source: PubMed

Speciation, Characterization, and Mobility of As, Se, and Hg in Flue Gas Desulphurization Residues

SOUHAIL R. AL-ABED,*,† GAUTHAM JEGADEESAN,‡ KIRK G. SCHECKEL,† AND THABET TOLAYMAT†

National Risk Management Research Laboratory, United States Environmental Protection Agency, 26 West Martin Luther King Drive, Cincinnati, Ohio 45268, and Pegasus Technical Services, 46 East Hollister Street, Cincinnati, Ohio 45219

Received October 1, 2007. Revised manuscript received December 13, 2007. Accepted January 02, 2008.

Flue gas from coal combustion contains significant amounts of volatile toxic trace elements such as arsenic (As), selenium (Se), and mercury (Hg). The capture of these elements in the flue gas desulphurization (FGD) scrubber unit has resulted in generation of a metal-laden residue. With increasing reuse of the FGD residues in beneficial applications, it is important to determine metal speciation and mobility to understand the environmental impact of its reuse. In this paper, we report the solid phase speciation of As, Se, and Hg in FGD residues using X-ray absorption spectroscopy (XAS), X-ray fluorescence spectroscopy (XRF), and sequential chemical extraction (SCE) techniques. The SCE results combined with XRF data indicated a strong possibility of As association with iron oxides, whereas Se was distributed among all geochemical phases. Hg appeared to be mainly distributed in the strong-complexed phase. XRF images also suggested a strong association of Hg with Fe oxide materials within FGD residues. XAS analysis indicated that As existed in its oxidized state (As(V)), whereas Se and Hg was observed in primarily reduced states as selenite (Se(IV)) and Hg(I), respectively. The results from the SCE and variable pH leaching tests indicated that the labile fractions of As, Se, and Hg were fairly low and thus suggestive of their stability in the FGD residues. However, the presence of a fine fraction enriched in metal content in the FGD residue suggested that size fractionation is important in assessing the environmental risks associated with their reuse.

Introduction

The fate and transport of toxic trace elements such as mercury (Hg), arsenic (As), and selenium (Se) emitted during coal combustion have received great attention because of stricter environmental regulations. The behavior of As, Se, and Hg during coal combustion and its partitioning in flue gas have been well-documented in literature (*1–6*). Volatile Hg is more likely to be emitted in the flue gas, whereas semivolatile As and Se are distributed among fly ash and flue gas. Examination of trace metal speciation in flue gases showed that Hg existed as Hg^{2+} and/or particulate Hg (Hg_p), whereas Se and As can exist in multiple oxidation states as Se(IV)/Se(VI) and As(III)/As(V) depending on the flue gas conditions. Additionally, As, Se, and Hg are also known to associate with fine particulate fly ash (*2, 4, 7*). Even though most electrostatic precipitators (ESP) remove 99% of the particulate emissions, their decreased efficiency in removing submicron particles can result in the escape of fine sized fly ash along with the flue gases (*5, 6*).

In an effort to reduce toxic pollutants along with SO_2 emissions from the flue gases, flue gas desulphurization (FGD) systems employ lime or limestone reagent as sorbents. During this process, lime converts to calcium sulfate ($CaSO_4 \cdot 2H_2O$, gypsum) and facilitates the capture of As, Se and Hg (*1, 6–9*). The residual material generated, otherwise called FGD residues, is either disposed or reused for beneficial purposes (*10, 11*). Investigation on the release of As, Se and Hg from FGD residues have shown that metal release under natural conditions (pH ~7) is not an environmental concern (*10–12*). The high alkalinity of the FGD material and the presence of As and Se in sparingly soluble calcium complexes ($CaSeO_3$ and $Ca_3As_2O_8$) results in low mobilities of the trace metals (*1, 2, 8, 9*). However, metal mobility can be significant at low and high pH conditions, especially for As and Se (*13, 14*). Additionally, the association of trace metals with the oxides and minerals present in fine particle fly ash and their subsequent capture in the FGD residues may change their mobility.

Since metal speciation and distribution in any solid define their toxicity and mobility, their determination is important to understand the environmental consequences of the reuse of FGD residues. In this study, we examine the speciation and mobility of As, Se and Hg in FGD residues using sequential chemical extraction (SCE) and synchrotron based spectroscopy techniques. X-ray absorption spectroscopy (XAS) and X-ray fluorescence spectroscopy (XRF) are frequently used to glean information on metal bonding and coordination in solid samples. Since the toxic metal concentrations in the FGD are fairly low and the solid matrix complex in nature, XAS and XRF studies would help provide molecular structure information that would help evaluate appropriate disposal and reuse scenarios of the FGD residue. In addition, we determine the release of the trace metals as a function of pH to examine the behavior of these metals under reuse or disposal scenarios.

Experimental Section

Sampling and Characterization. Multiple samples of FGD residues were obtained from different power plants located in Pennsylvania. The FGD samples (<125 μm mean particle size) had a moisture content of about 25%. The samples, designated here forth as FGD S11, S9, and S7, were subjected to EPA Method 3051 in triplicate to determine "environmentally available" elements (*15*). National Institute of Standards and Technology (NIST) references, NIST 1633B and NIST 2710, were used as quality control for As, Se, and Hg. X-ray diffraction (XRD, Phillips PW3040/00 X'Pert-MPD Diffractometer) analysis was performed on bulk FGD and the diffraction pattern was analyzed to identify the crystalline phases.

As mentioned earlier, a fine sized particulate fly ash fraction enriched in trace metals, escaping the ESPs, may be captured in the FGD residues. To determine the possible enrichment of metals in such a fraction, we employed a simple density separation procedure by stirring 200 g of bulk FGD residue in 0.5 L of deionized water (*7*). Two distinct

* Corresponding author phone: (513) 569-7849; fax: (513) 569-7879; e-mail: al-abed.souhail@epa.gov.
† U.S. EPA.
‡ Pegasus Technical Services.

10.1021/es702479n CCC: $40.75
Published on Web 01/25/2008

TABLE 1. Environmentally Available Metal Content in FGD residues obtained by EPA Method 3051[a]

metal content (mg/kg)	FGD S11	FGD S9	FGD S7	FGD S9 LF	FGD S9 HF
As	4.9 ± 0.1	8.6 ± 0.5	5.6 ± 1.0	86.8 ± 14.1	8.2 ± 0.2
Se	18.4 ± 2.3	9.2 ± 0.9	9.7 ± 2.7	96.4 ± 12.1	8.9 ± 1.0
Fe	1174.1 ± 138	3859.0 ± 233	2184.3 ± 602	24789.9 ± 534	3278.7 ± 235
Hg	2.3 ± 0.2	1.4 ± 0.1	1.0 ± 0.1	115.4 ± 1.0	1.1 ± 0.1

[a] All concentrations (mean ± SD) are reported on a dry weight basis.

fractions were observed, with a dark colored fraction of the material floating in the reactor and a white denser fraction settled in the bottom. The floating fraction (designated light fraction (FGD LF)) and the denser fraction (designated heavy fraction (FGD HF)) were separated using vacuum suction, freeze-dried, and analyzed for total metals using EPA Method 3051.

Sequential Chemical Extractions. Two separate sequential chemical extraction (SCE) procedures, modified slightly from Tessier et al. (*16*) and Kim et al. (*17*), were employed to identify associations of As, Se, and Hg in the FGD residues (see Tables S1 and S2 in the Supporting Information for details). At the end of each extraction procedure, the extract was centrifuged, filtered through 0.45 μm Nylon filters (Fisher Scientific, Fair Lawn, NJ) and analyzed for metal concentration. Prior to each extraction step, the solid samples were freeze-dried to remove moisture and also minimize solid losses.

XAS Data Collection. Because all the FGD samples were similar in character, a representative sample with higher As, Se, and Hg content was analyzed by XAS to examine the solid phase speciation. Preliminary work on the bulk FGD provided poor spectra due to low metal concentrations in the sample. Therefore, further analysis was done using the light fractions (FGD LF), which was enriched in As, Se, and Hg (data discussed below). Arsenic K-edge (11 867 eV), selenium K-edge (12 658 eV), and mercury L_{III} absorption edge (12 284 eV) XAS spectra and XRF distribution of metals were collected using the MR-CAT beamline at the Advanced Photon Source (APS) at Argonne National Laboratory (ANL, Argonne, IL). The APS electron storage ring operated at 7 GeV with a topup fill status. All spectra were collected in fluorescence mode with Si (111) double-crystal monochromator. For each sample, multiple scans were collected and averaged to improve the signal-to-noise ratio. Arsenic and selenium spectra were collected from bulk samples while Hg XAS were collected from hotspots identified in XRF elemental maps. A series of reference standards and model compounds were used to obtain the reference standard spectra and compare the associations of As, Se, and Hg in the FGD residues. XRF data were collected with a 20 μm spot size focused with KB mirrors. The samples were mounted on the rotation axis of an $x-y-\theta$ stepping-motor stage for XRF experiments.

XAS Data Analysis. The quantitative X-ray absorption near edge structure (XANES) analysis was performed using ATHENA. Data reduction was done in a standard manner including data averaging, background subtraction with the linear function through the pre-edge region (*18–20*). The Extended X-ray absorption fine structure (EXAFS) data obtained was converted to frequency (k) space and weighted by k^2 for As and k^3 for Se. The generated Fourier transformed (FT) and the radial structure–functions (RSF) were then used for data fitting.

Experimental EXAFS data were fitted with single-scattering theoretical phase and amplitude functions calculated with the ab initio computer code FEFF6 and ARTEMIS on the basis of input files of known minerals (*18*). The parameters determined were coordination number (CN), interatomic distance (R), and the Debeye-Waller parameter (σ^2). The amplitude reduction factor (S_0^2) was fixed at 0.9 for As and 0.95 for Se and the energy offset (ΔE_0) was determined by fitting the As−O and Se−O first-shell peaks. Then, ΔE_0 was fixed for all the subsequent fits and the CN, R, and σ^2 were determined. Finally, the fitted parameters were used to model the unfiltered EXAFS function. Error estimates of the fitted parameters were R ± 10%, CN ± 20%, and σ^2 ± 20%.

Constant pH Extraction Tests. Extraction tests at constant pH values between 3 and 11 were performed. The test conditions used 50 g of FGD sample added to 1000 mL of deionized water buffered with 4 g/L $NaHCO_3$, adjusted to a definite pH. The duration of the experiment was 48 h.

Analysis. The extract As, Fe, and Se concentrations were analyzed using inductively coupled plasma-atomic emission spectrometry (ICP-AES, IRIS Intrepid, Thermo Electron Corporation, CA; EPA Method 6010B). The instrument detection limits for As, Se and Fe were 12, 10, and 58 μg/L, respectively. The total Hg content was determined by EPA Method (7473), using thermal decomposition amalgamation followed by atomic absorption spectrometry (Milestone, Inc.). The detection limit for Hg was 1 ng.

Results and Discussion

Characteristics of FGD Residues. The concentration of the elements of concern, As, Se and Hg, varied with the FGD sample (Table 1). The data showed that arsenic concentrations were the highest in FGD S9 sample (8.6 mg/kg), while Se was higher in the S11 sample (18.4 mg/kg). Hg content was within 1–2.3 mg/kg in the FGD samples, typical of FGD residues. XRD analysis on bulk FGD revealed calcium sulfate ($CaSO_4$) as the predominant crystalline phase. Other less intense peaks appeared to be those for Illite and ferrihydrite (FeOOH). These results were confirmed by Mössbauer spectroscopy which identified Fe speciation as 85% ferrihydrite and 15% Fe (III) in clay structures (data not shown). The presence of FeOOH can be attributed to the capture of particulate fly ash (composed of clay minerals and hematite) during the scrubbing process (*11, 12, 21, 22*).

The density separation procedure provided two distinct fractions with the lighter fraction less than 0.01 wt% of the total FGD sample added. The metal content (Table 1) indicated that the floating fraction (FGD LF) was enriched almost 10-fold for As (86.8 mg/kg), Se (96.4 mg/kg) and Fe, while Hg (115.4 mg/kg) was concentrated almost 100 times. Compared to the original FGD S9 sample, As and Se content decreased marginally (3–5%) in the denser fraction (FGD HF). The decrease in Hg and Fe content was almost 15–20%. Even though a detailed characterization of the fines could not be performed, it is believed that they could possibly occur in the FGD as a result of the capture of particulate matter escaping the ESPs. It has been reported in previous studies that the concentrations of volatile As, Se and Hg in the particles leaving the ESPs are higher in the medium to fine fractions (106–10 μm) (*2, 4, 5, 23, 24*). As the flue gas temperature decreases along the combustion process, the fine particles act as condensation nuclei for the volatile elements, thereby enriching their concentrations. Guo et al. (*2*) have reported that arsenic is enriched in the particulate fly ash. With more than 83% of volatile Hg in the flue gas (*3*) and the possibility of Hg capture on iron oxide on the surface

TABLE 2. As, Se, Fe, and Hg Distribution in FGD Residues, Along with Percent Distribution among the Extracted Phases

extraction Step	extracted phase	As (%)	Se (%)	Fe (%)
S1	water soluble	0.9 ± 0.0	1.9 ± 0.1	0.0 ± 0.0
S2	exchangeable	2.0 ± 0.5	6.7 ± 0.5	0.0 ± 0.0
S3	carbonate	15.2 ± 0.0	25.4 ± 5.1	1.4 ± 0.1
S4	amorphous Fe, Mn oxides	53.0 ± 7.4	36.3 ± 7.4	50.7 ± 7.7
S5	crystalline Fe, Mn oxides	3.7 ± 0.0	2.2 ± 0.3	3.7 ± 0.5
S6	organic matter	0.9 ± 0.0	16.3 ± 2.7	0.0 ± 0.0
S7	residual	24.4 ± 2.6	11.2 ± 1.3	44.2 ± 2.2
	% recovery	78.17	115.58	64.88

extraction step	Extracted phase	Hg (%)
F1	water soluble	0.31 ± 0.02
F2	human stomach acid soluble	0.06 ± 0.01
F3	organic matter	0.04 ± 0.00
F4	strong complexed (Hg^0)	72.28 ± 9.36
F5	residual	27.32 ± 5.05
	% recovery	53.77

[a] The % distributions among the extracted phases were calculated as the ratio of metal concentration (mg/kg) extracted in each phase to the sum of all extracted phases. The % recovery provided was the ratio of the sum of extracted phases to the total available content.

of the fly ash particle escaping the ESPs, Hg enrichment can be expected.

As, Se, and Fe SCE Distribution in FGD Residues. The percent distribution of As, Se and Fe in the bulk FGD S9 sample among the different extraction steps is provided in Table 2. This sample was selected as it contained a representative amount of the target metals. The extraction procedure could not be performed on FGD LF as the generated amounts were very low. Percent metal recoveries, calculated as the ratio of sum of all fractions to the total environmentally available content, were observed to be reasonable (Table 2).

Arsenic was predominantly partitioned in the Fe-associated fractions (sum of S4 and S5 fractions) compared to the other labile fractions. The release of almost 50% of Fe in the amorphous Fe-oxides (S4) fraction was also observed. It has been observed in previous studies that arsenic existed in the form of calcium arsenates in the FGD residues (*1, 8*). The elevated arsenic release in this fraction could occur due to the acidic dissolution of Ca-associated fractions (*26*). Despite the lack of selectivity and the ambiguity in distinguishing As distributions in Fe and Ca-associated fractions, the results indicated limited arsenic mobility from FGD residue because of its incorporation in more stable S4 and S5 fractions. Twenty-five percent of the environmentally available As was released from the residual phase, whereas the more labile forms (sum of the first three fractions) were low, accounting for 18% for total As.

Substantial amounts of Se were released in all steps with the solid-phase solubility following the order: water soluble (S1) = crystalline Fe oxides (S5) < exchangeable (S2) < residual (S7) < organic matter (S6) < carbonate (S3) < amorphous Fe oxides (S4). Similar to As, Se association with Fe-oxide fractions was higher (38%), compared to the carbonate (25%) and residual (11%) fractions. Some of the apparent Se release in the S6 fraction is attributable due to desorption at alkaline pH, rather than any association with organic matter. It has been reported that Se(IV) associated with amorphous Fe-oxide can readsorb into other minerals. The subsequent use of oxidative extractant such as sodium hypochlorite may oxidize Se(IV) to Se(VI) and release from solution at alkaline pH (*27*). Labile Se was observed to be higher (34%).

Hg SCE Distribution in FGD Residues. Even though the selective extraction procedure for Hg has been widely reported to be successful (*17, 28*), Hg recoveries in the FGD residues were observed to be very low, probably because of low extract concentrations (Table 2). It has been noted in previous research that the first three fractionation steps can be ambiguous at low Hg concentrations. Nevertheless, the data indicated that Hg in the FGD residue was the highest in the F4 fraction (72%), representing Hg^0. It should, however, be noted that other classes of Hg such as Hg (I) and Hg associated with Fe-oxides can be extracted in this fraction. Because Hg in the flue gas is more likely to be in the form of Hg (I), Hg (II), or Hg_p (*3–6, 20*), their elevated release in the F4 fraction is expected. Besides the F4 fraction, the residual fraction indicating mercuric sulfide accounted for almost 28% of total Hg extracted. The first two sequentially extracted fractions, F1 and F2, corresponding to the water-soluble and human stomach acid soluble Hg, respectively, were very low. The results suggested that the bioavailable and labile Hg fractions with high environmental risks were low and thus indicated the stability of Hg in FGD residue. The % Hg recovery in the NIST 2710 standard was higher (70%) and the extraction profile was similar to that reported previously (*28*), albeit at lower amounts (data not shown).

As K-Edge XAS Analysis. As mentioned earlier, due to poor XAS spectra on the bulk FGD residue, only the light fraction (FGD LF) was analyzed. Arsenic XANES data for the FGD LF, along with As(III) and As(V) standards, Realgar (As(III) sulfide), and As-treated Fe-oxide, are illustrated in Figure S1 in the Supporting Information. Analysis of the XANES first derivative curves resulted in an absorption edge shift of 5 eV between As(III) and As(V) species. The XANES and corresponding first derivative plots for FGD LF showed absorption maxima at 11876 eV, similar to As(V) standards As(V)-treated Fe-oxide. The As(III) standards and Realgar showed the absorption maxima at 11872 eV, characteristic of As(III) species.

The Fourier transformed $k^2\chi(k)$ and the corresponding radial structure–function (RSF) for FGD LF and As Fe-oxide samples are shown in Figure 1. The fits of the theoretical expressions (solid lines) are also shown and the parameters deduced are listed in Table 3. The fit results on FGD LF revealed that the As−O first shell peak at an average interatomic distance of 1.73 Å was composed of an average CN of 3.69 atoms, which was diagnostic for As (V) species. The second shell in the FT plots for FGD LF is due to the As-Fe correlations of 1.8 Fe atoms at 3.50 Å. The As (V)-treated Fe oxide fit results corresponded closely with previous literature, with As-O shell of 4.18 oxygen atoms at 1.70 Å and

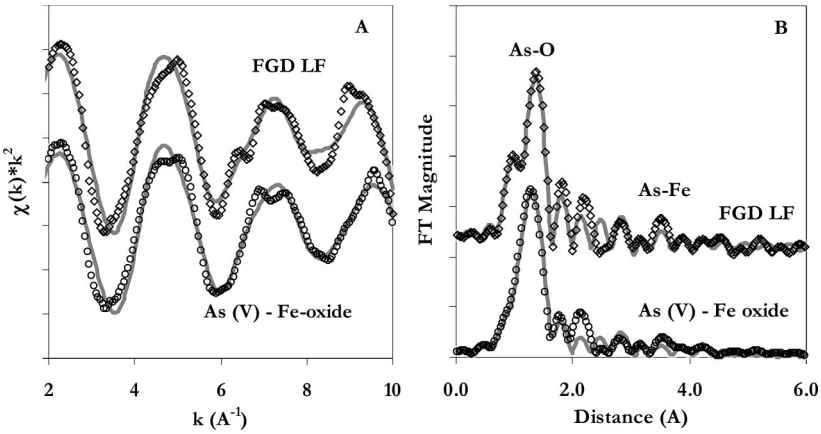

FIGURE 1. K^2 weighted observed (dotted line; (top, FGD LF; bottom, As sorbed on Fe-oxide)) and model calculated (solid line; (top, FGD LF; bottom, As sorbed on Fe-oxide)) As K-edge EXAFS spectra (A) and Fourier transform magnitude (B).

TABLE 3. EXAFS Fit Parameter Results for As Speciation FGD Light Fraction (FGD LF) and As(V) Sorbed on Iron Oxides[c]

sample	interatomic shell	CN	R (Å)	σ^2 (Å^{-1})	ΔE_0
FGD light fraction (FGD LF)	As−O	3.69	1.73	0.0007	12.63
	As−Fe	1.80	3.50	0.0096	12.63
As (V) sorbed on Fe oxide	As−O	4.18	1.70	0.0031	9.76
	As−Fe	1.80	3.36	0.0136	9.75
		References			
fly ash sample[b]	As−O	4.10	1.70		
As (V) sorbed on α-FeOOH	As−O	4.00	1.70	0.0006	
	As−Fe	2.00	3.36	0.0005	

[a] CN = coordination number, R = interatomic distance, σ^2 = Debeye−Waller parameter, and ΔE_0 = threshold energy shift in eV. [b] Data reported by Huggins et al. (*30*). [c] Data reported by Manning et al (*29*).[a]

the As-Fe shell of 1.8 Fe atoms at 3.50 Å (*29*). The distance and the coordination number obtained for the FGD LF fits indicated the presence of As(V) surface complex attached to the Fe structure, which was in agreement with previous publications (*22, 30*). These results combined with XRF analysis and sequential extraction data provided a strong indication of arsenic association with Fe oxide.

Se K-Edge XAS Analysis. Selenium XANES data and the corresponding first derivative curves for the FGD LF are illustrated in Figure S2 in the Supporting Information. The XANES data and the first derivative plot for FGD LF indicated the predominant presence of Se (IV) as the major species. Previous literature (*1, 9, 31*) has shown that SeO_2 was the major selenium species in the flue gas, which combines with lime during scrubbing to form $CaSeO_3$. Se (IV) species are usually more dominant in fly ash samples, even though evidence of Se(VI) in others was also observed (*30*). The similarities between the first derivative curves for our model compound ($CuSeO_3$) leads us to believe that Se(IV) was the major species in the FGD LF fraction. A closer inspection of the XANES spectral data for FGD LF indicated a small shoulder, corresponding to Se(VI) suggesting that selenates may also be present, albeit in a minor fraction. No evidence of Se(IV) oxidation by the X-ray beam was observed.

The Fourier transformed $k^3\chi(k)$ and the corresponding radial structure–function (RSF) for FGD LF sample and $CuSeO_3$ sample along with the fits of the theoretical expressions (solid lines) are shown in Figure 2. The parameters deduced from the fits are listed in Table 3. The fit results on FGD LF revealed that the EXAFS was dominated by scattering of the first Se−O coordination shell. The results on the fitting FGD LF EXAFS data indicated that the Se−O shell at an interatomic distance of 1.68 Å was composed of an average CN of 3.38 oxygen atoms, consistent with Se(IV) species. The fit results corresponded well with previous literature (*30, 32*). The lack of proper fit of the second shell, possibly Se−Fe at around 3 Å could probably either due to the formation of outersphere complex with Fe (*32*) or the absence of any Se association with Fe oxide. The lack of any definitive determination of Se association with the Fe in the FGD indicates that Se extracted in the Fe-oxide phase in the sequential extraction may possibly be due to the release of Ca-selenates.

Hg X-ray Absorption and X-ray Fluorescence Spectroscopies. The elemental distribution of Hg was measured by XRF for the FGD S9 LF sample. Since the focus of these experiments was Hg (L_{III} 12284 eV), Fe and As fluorescence were able to be measured congruently with Hg information; however, Se (K 12658 eV) was above the energy utilized in the XRF data collection (Figure S3). Iron, arsenic, and mercury distribution shows a very strong correlation of Hg and As to Fe (Figure S4 in the Supporting Information) for the 700 μ m by 400 μm scan area. Noted in Figure S3 are locations where Hg XANES data were collected. Figure 3A shows the corresponding XANES spectra for points collected from the Hg XRF map (Figure S3) in addition to Hg standards of Hg(II) sorbed to ferrihydrite and Hg(I) chloride. As reported previously in the literature, Hg(II) compounds tend to have a more defined pre-edge peak at about 12284 eV, whereas Hg(I) phases exhibit a less distinct pre-edge shoulder. By this comparison, it appears that the oxidation state of Hg in the FGD samples is Hg(I). Hg speciation can also be determined by first derivative XANES peak separation (in eV), also known as the inflection point difference (IPD), which can be used as an indicator of the local structure and bonding chemistry of Hg (*19*). The IPD value for the FGD material is 9.97 eV and falls between IPD values for Hg (II) sorbed to ferrihydrite (10.4 eV) and Hg (I) chloride (8.00 eV) (Figure 3B). Published IPD values for Hg standards indicate $Hg(I)_2SO_4$ (9.6 eV) (*19*) is similar to the FGD values. However, the strong XRF correlation of Hg to Fe suggests Hg (I) binding to Fe oxides yet sulfate bridging on Fe oxide surfaces cannot be ruled out but likely does not fit the observed stability of Hg

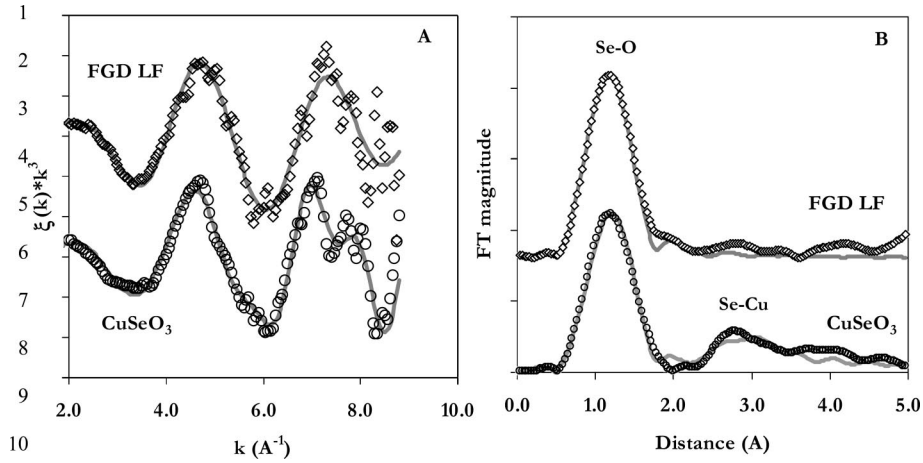

FIGURE 2. k^3 weighted observed (dotted line; (top-FGD LF, bottom-$CuSeO_3$)) and model calculated (solid line; (top-FGD LF, bottom-$CuSeO_3$)) Se K-edge EXAFS spectra (A) and Fourier transform magnitude (B).

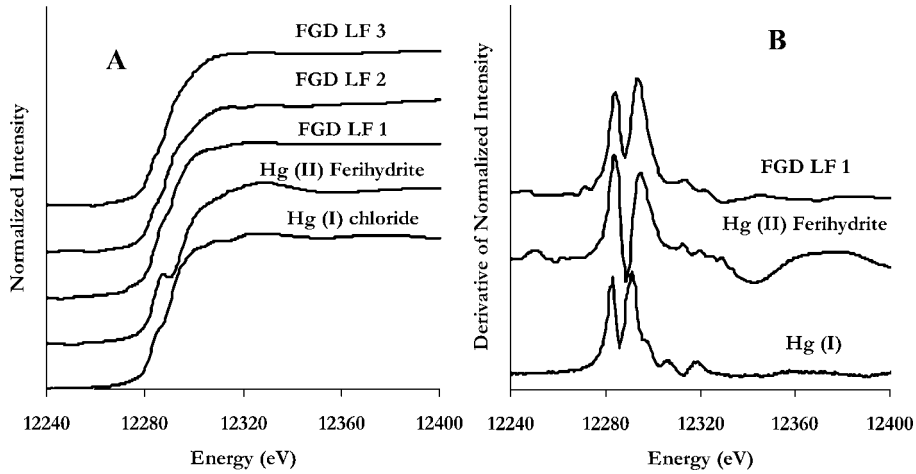

FIGURE 3. Mercury XANES spectra (panel A) and derivative of XANES spectra (panel B) for FGD LF and reference standards.

TABLE 4. EXAFS Fit Parameter Results for Se speciation FGD Light Fraction (FGD LF) and $CuSeO_3$[a]

sample	interatomic shell	CN	R (Å)	σ^2>(Å^2)	ΔE_0
FGD light fraction (FGD LF)	Se−O	3.38	1.68	0.0018	9.15
	Se−Fe				
$CuSeO_3$	Se−O	2.94	1.70	0.0005	8.56
	Se−Cu	1.75	3.16	0.0005	8.56
	References				
fly ash sample[b]	Se-O	2.8–3.1	1.69–1.72	0.0028	8.9–12.0
Se (IV) sorbed on hydrous aluminum oxide[c]	Se-O	2.5–3.4	1.70	0.0020	12.9
	Se-Al	3.2	1.2–1.9	0.0050	12.9

[a] CN = coordination number, R = interatomic distance, σ^2 = Debeye-Waller parameter and ΔE_0 = threshold energy shift in eV. [b] Data reported by Huggins et al. (*30*). [c] Data reported by Peak (*32*).

retention in the FGD samples. There is no reported IPD value for Hg(I) sorption on Fe oxides in the literature.

Environmental Implications of FGD Reuse and Disposal. The XAS spectroscopy and the sequential extraction results indicated that As, Se and Hg existed as As(V), Se(IV), and Hg(I), respectively, and can be released in natural environments. The association of the metals with either iron oxide or calcium complexes provided stability and thereby reduced their labile fractions in bulk FGD. Leaching tests at different pH conditions (see Figure S5 in the Supporting Information for details) indicated that Hg leached higher at acidic pH. Hg appeared to be fairly stable in the FGD, with maximum release at pH of 1.2 (0.38 mg/kg), tapering to almost 0.1 mg/kg between pH 5–11. On the other hand, As leaching profile was observed to be amphoteric with higher leaching at low (0.13 mg/kg; 1.8%) and high pH (0.33 mg/kg; 5.6%), typical of arsenic bearing solids (*13*). However, under highly alkaline conditions (pH 11), As release was drastically reduced, probably because of its encapsulation on coprecipitating calcium and/or iron hydroxides (*7, 33, 34*). In the acidic pH range, Se release was lower (0.12 mg/kg; 1.4%). As pH increased, higher Se release was observed increasing to almost 0.48 mg/kg (5.6%) at pH 11, consistent with Se desorption from solid matrices. The corresponding aqueous extract concentrations were well below EPA mandated limit, similar to previously reported literature (*10, 14, 33*). The data also showed that metal release correlated strongly with the more mobile fractions in the sequential extraction data. For example, As release at pH 9 was higher than S1 and S2 fractions, whereas Se was within the percent extracted from

S1 and S2 fractions. This indicated that the more stable forms of trace metals are unlikely to leach even at extreme pH conditions. Despite the identification of fairly stable species of As and Se and their apparent association with stable iron oxide, the separation of fine particles from the bulk FGD residue poses an serious environmental risk. For example, in addition to reuse application in construction wallboard, FGD material has been touted for agricultural benefits to add Ca to soils without increases to soil pH. With a metal-enriched fraction that floats readily in water, potential runoff during rainfall events may be an issue for land application of FGD residues. In light of such concerns, the reuse of FGD should be carefully evaluated.

Acknowledgments

This research was performed at and funded by the National Risk Management Research Laboratory of the U.S. Environmental Protection Agency. This paper has not been subjected to the Agency's internal review. Therefore, the research results presented herein do not, necessarily, reflect the views of the Agency or its policy. MRCAT operations are supported by the Department of Energy and the MRCAT member institutions.

Supporting Information Available

Details of the sequential chemical extractions (SCE) for As, Se (Table S1) and Hg (Table S2), XANES spectra on As in FGD samples (Figure S1), Se in FGD samples (Figure S2), XRF maps showing distribution of Fe, Hg, and As in FGD samples and points of Hg XAS spectra (Figure S3), correlation plots of Fe versus Hg and As XRF mapping data (Figure S4), and As, Se, and Hg release as a function of pH (Figure S5) (PDF). This material is available free of charge via the Internet at http://pubs.acs.org.

Literature Cited

(1) Diaz-Somoano, M.; Martinez-Tarazona, M. R. Retention of arsenic and selenium compounds using limestone in a coal gasification flue gas. *Environ. Sci. Technol.* **2004**, *38* (3), 899–903.
(2) Guo, X.; Zheng, C. G.; Xu, M. H. Characterization of arsenic emissions from a coal-fired power plant. *Energy Fuels* **2004**, *18* (6), 1822–1826.
(3) Guo, X.; Zheng, C. G.; Xu, M. H. Characterization of mercury emissions from a coal-fired power plant. *Energy Fuels* **2007**, *21* (2), 898–902.
(4) Otero-Rey, J. R.; Lopez-Vilarino, J. M.; Moreda-Pineiro, J.; Alonso-Rodriguez, E.; Muniategui-Lorenzo, S.; Lopez-Mahia, P.; Prada-Rodriguez, D. As, Hg, and Se flue gas sampling in a coal-fired power plant and their fate during coal combustion. *Environ. Sci. Technol.* **2003**, *37* (22), 5262–5267.
(5) Pavageau, M. P.; Pecheyran, C.; Krupp, E. M.; Morin, A.; Donard, O. F. X. Volatile metal species in coal combustion flue gas. *Environ. Sci. Technol.* **2002**, *36* (7), 1561–1573.
(6) Pavlish, J. H.; Sondreal, E. A.; Mann, M. D.; Olson, E. S.; Galbreath, K. C.; Laudal, D. L.; Benson, S. A. State review of mercury control options for coal-fired power plants. *Fuel Process. Technol.* **2003**, *82* (2–3), 89–165.
(7) Taerakul, P.; Sun, P.; Golightly, D. W.; Walker, H. W.; Weavers, L. K. Distribution of arsenic and mercury in lime spray dryer ash. *Energy Fuels* **2006**, *20* (4), 1521–1527.
(8) Jadhav, R. A.; Fan, L. S. Capture of Gas-Phase Arsenic Oxide by Lime: Kinetic and Mechanistic Studies. *Environ. Sci. Technol.* **2001**, *35* (4), 794–799.
(9) Ghosh-Dastidar, A.; Mahuli, S.; Agnihotri, R.; Fan, L. S. Selenium Capture Using Sorbent Powders: Mechanism of Sorption by Hydrated Lime. *Environ. Sci. Technol.* **1996**, *30* (2), 447–452.
(10) *Managing Coal Combustion Residues in Mines*; National Research Council of the National Academies: Washington, D.C., 2006.
(11) Kairies, C. L.; Schroeder, K. T.; Cardone, C. R. Mercury in gypsum produced from flue gas desulfurization. *Fuel* **2006**, *85* (17–18), 2530–2536.
(12) Kost, D. A.; Bigham, J. M.; Stehouwer, R. C.; Beeghly, J. H.; Fowler, R.; Traina, S. J.; Wolfe, W. E.; Dick, W. A. Chemical and physical properties of dry flue gas desulfurization products. *J. Environ. Qual.* **2005**, *34* (2), 676–686.
(13) Al-Abed, S. R.; Jegadeesan, G.; Purandare, J.; Allen, D. Arsenic release from iron rich mineral processing waste: Influence of pH and redox potential. *Chemosphere* **2007**, *66* (4), 775–782.
(14) Taerakul, P.; Sun, P.; Golightly, D. W.; Walker, H. W.; Weavers, L. K.; Zand, B.; Butalia, T.; Thomas, T. J.; Gupta, H.; Fan, L.-S. Characterization and re-use potential of by-products generated from the Ohio State Carbonation and Ash Reactivation (OSCAR) process. *Fuel* **2007**, *86* (4), 541–553.
(15) *Test Methods for Evaluating Solid Waste, Physical/Chemical Methods*; U.S. Environmental Protection Agency: Washington, D.C., 1997, SW-846.
(16) Tessier, A.; Campbell, P. G. C.; Bisson, M. Sequential Exctraction Procedure for Particulate Trace Metals. *Anal. Chem.* **1979**, *51* (7), 884–851.
(17) Kim, C. S.; Bloom, N. S.; Rytuba, J. J.; Brown, G. E. Mercury speciation by X-ray absorption fine structure spectroscopy and sequential chemical extractions: A comparison of speciation methods. *Environ. Sci. Technol.* **2003**, *37* (22), 5102–5108.
(18) Ravel, B.; Newville, M. ATHENA, ARTEMIS, HEPHAESTUS: data analysis for X-ray absorption spectroscopy using IFEFFIT. *J. Synchrotron Radiat.* **2005**, *12*, 537–541.
(19) Hutson, N. D.; Attwood, B. C.; Scheckel, K. G. XAS and XPS characterization of mercury binding on brominated activated carbon. *Environ. Sci. Technol.* **2007**, *41* (5), 1747–1752.
(20) Huggins, F. E.; Yap, N.; Huffman, G. P.; Senior, C. L. XAFS characterization of mercury captured from combustion gases on sorbents at low temperatures. *Fuel Process. Technol.* **2003**, *82* (2–3), 167–196.
(21) Querol, X.; Alastuey, A.; Lopez-Soler, A.; Mantilla, E.; Plana, F. Mineral composition of atmospheric particulates around a large coal-fired power station. *Atmos. Environ.* **1996**, *30* (21), 3557–3572.
(22) Zielinski, R. A.; Foster, A. L.; Meeker, G. P.; Brownfield, I. K. Mode of occurrence of arsenic in feed coal and its derivative fly ash, Black Warrior Basin, Alabama. *Fuel* **2007**, *86* (4), 560.
(23) Galbreath, K. C.; Toman, D. L.; Zygarlicke, C. J.; Pavlish, J. H. Trace element partitioning and transformations during combustion of bituminous and subbituminous U.S. coals in a 7-kW combustion system. *Energy Fuels* **2000**, *14* (6), 1265–1279.
(24) Pavageau, M. P.; Morin, A.; Seby, F.; Guimon, C.; Krupp, E.; Pecheyran, C.; Poulleau, J.; Donard, F. X. Partitioning of metal species during an enriched fuel combustion experiment. Speciation in the gaseous and particulate phases. *Environ. Sci. Technol.* **2004**, *38* (7), 2252–2263.
(25) Senior, C. L.; Johnson, S. A. Impact of carbon-in-ash on mercury removal across particulate control devices in coal-fired power plants. *Energy Fuels* **2005**, *19* (3), 859–863.
(26) Mihaljevič, M.; Poňavič, M.; Ettler, V.; Šebek, O. A comparison of sequential extraction techniques for determining arsenic fractionation in synthetic mineral mixtures. *Anal. Bioanal. Chem.* **2003**, *377* (4), 723–729.
(27) Gleyzes, C.; Tellier, S.; Astruc, M. Fractionation studies of trace elements in contaminated soils and sediments: a review of sequential extraction procedures. *TrAC Trends Anal. Chem.* **2002**, *21* (6–7), 451–467.
(28) Bloom, N. S.; Preus, E.; Katon, J.; Hiltner, M. Selective extractions to assess the biogeochemically relevant fractionation of inorganic mercury in sediments and soils. *Anal. Chim. Acta* **2003**, *479* (2), 233–248.
(29) Manning, B. A.; Hunt, M. L.; Amrhein, C.; Yarmoff, J. A. Arsenic(III) and Arsenic(V) Reactions with Zerovalent Iron Corrosion Products. *Environ. Sci. Technol.* **2002**, *36* (24), 5455–5461.
(30) Huggins, F. E.; Senior, C. L.; Chu, P.; Ladwig, K.; Huffman, G. P. Selenium and Arsenic Speciation in Fly Ash from Full-Scale Coal-Burning Utility Plants. *Environ. Sci. Technol.* **2007**, *41* (9), 3284–3289.
(31) Yan, R.; Gauthier, D.; Flamant, G.; Wang, Y. Behavior of selenium in the combustion of coal or coke spiked with Se. *Combust. Flame* **2004**, *138* (1–2), 20–29.
(32) Peak, D. Adsorption mechanisms of selenium oxyanions at the aluminum oxide/water interface. *J. Colloid Interface Sci.* **2006**, *303* (2), 337–345.
(33) Jankowski, J.; Ward, C. R.; French, D.; Groves, S. Mobility of trace elements from selected Australian fly ashes and its potential impact on aquatic ecosystems. *Fuel* **2006**, *85* (2), 243.
(34) van der Hoek, E. E.; Comans, R. N. J. Modeling Arsenic and Selenium Leaching from Acidic Fly Ash by Sorption on Iron (Hydr)oxide in the Fly Ash Matrix. *Environ. Sci. Technol.* **1996**, *30* (2), 517–523.

ES702479N